Fault-Tolerant Computing with Single Qudit Encoding

M. Mezzadri[†], ^{1,2} A. Chiesa[†], ^{1,2,3} L. Lepori, ^{1,2} and S. Carretta^{1,2,3,*}

¹ Università di Parma, Dipartimento di Scienze Matematiche, Fisiche e Informatiche, I-43124, Parma, Italy
² Gruppo Collegato di Parma, INFN-Sezione Milano-Bicocca, I-43124 Parma, Italy
³ UdR Parma, INSTM, I-43124 Parma, Italy

We present a general approach for the Fault-Tolerant implementation of stabilizer codes with a logical qubit encoded into a single multi-level qudit, preventing the explosion of resources of multi-qubit codes. The proposed scheme allows for correction and universal quantum computation. We demonstrate its effectiveness by simulations on molecular spin qudits, finding an almost exponential suppression of logical errors with the qudit size. The resulting performance on a small qudit is remarkable when compared to qubit codes using thousands of units.

A "useful" quantum computer should be universal, accurate and scalable [1], i.e. capable to solve any kind of problem with an arbitrary small error and with resources which do not increase exponentially with the size of the problem or with the target error. Meeting these conditions on a noisy hardware requires a Fault-Tolerant (FT) quantum error correction (QEC) approach, which allows for universal quantum computation (QC) with an arbitrary error reduction, while remaining experimentally achievable. In practice, an elegant mathematical construction must be combined with a feasible physical implementation.

The standard way to tackle this problem relies on encoding the elementary unit of computation (a logical qubit, LQ) into a collection of distinct physical qubits [2–6]. In principle, this allows one to design QEC codes suppressing the error on the LQ compared to the elementary error probability (p) on each physical qubit, thus meeting FT for p below a certain threshold. Moreover, the error can be further reduced by a concatenated encoding, i.e. by increasing the number of physical qubits in the LQ [3, 7]. However, FTQC also demands a recipe to implement all the required *gadgets* (error correction, gates, measurements) without ever amplifying errors. This comes usually with an enormous cost in the number of physical qubits, required not only for the encoding, but also as ancillae for the various computational steps [7]. Different codes were developed along these lines, with increasingly higher threshold [8–12, 14–17, 83], but for all of them the most important road-block to an actual implementation remains the explosion in the number of physical qubits and gates for a reliable algorithm [18, 19, 83]. For instance, Fig. 1-(a) shows the circuit for a logical gate X_L followed by FT error correction (EC) using the fivequbit code [20], i.e. the smallest code correcting a generic one-qubit error. Even this compact encoding requires 25 qubits (5 to encode the logical state $|\psi\rangle + 20$ ancillae) to achieve FTQC [10]. Moreover, to increase the correcting power (i.e. to tolerate more than a single error) a concatenation strategy is usually followed [Fig.1-(b)] [7], which recursively encodes a LQ into 5 lower-level units,

thus quickly resulting in a dramatic increase of physical resources.

Here we pursue an alternative approach [Fig. 1-(c)] based on embedding a LQ into a *single* multi-level quantum system [21, 22] (a *qudit*), which is then corrected and operated in a FT manner. Along this line, cat and binomial codes in superconducting circuits and microwave modes [23–25] or molecular spin systems [22, 26–29] have been recently proposed, reaching in some cases the break-even point [30] and supporting "transparent" gates [31, 32] and error detection [33] with no error propagation [24, 34]. However, a FT implementation with error suppression to an arbitrary level must still be fully explored [24].

In our FT qudit approach (FTqd), an almost exponential error reduction comes only with a linear growth in the number of qudit levels, without increasing the complexity of the LQ with additional objects. This extremely simplifies the actual control of the hardware and could make the

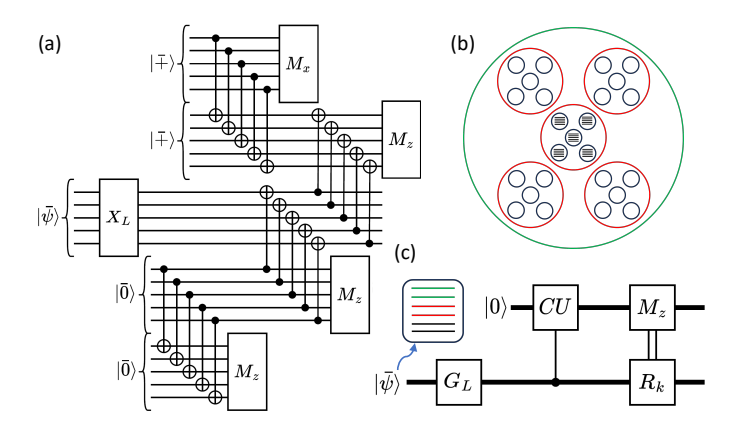


Figure 1: Comparison between the FT circuit implementing a single-qubit logical gate and the consequent EC for (a) the five-qubit code with Steane EC and (c) our FTqd embedding a LQ into a single multi-level qudit (bold lines). The bar over $|\psi\rangle$ indicates this is an encoded logical state. While in (a) 25 qubits are needed to correct a single error and their number increases in a concatenated encoding (b), in (c) only 2 qudits suffice, with higher-order correction achieved by only adding a few levels.

^{*} stefano.carretta@unipr.it

FTqd a viable path towards the physical implementation of a "useful" quantum computing machine. We illustrate a stabilizer code allowing us to fault-tolerantly encode and process quantum information in a d-levels qudit. In particular, we show that errors can be detected and corrected by measuring stabilizer operators on a d/2-levels ancilla. Moreover, we show how to implement a universal set of logical single and two-qubit gates, only relying on the proper connectivity between the different eigenstates defining the LQ. As an example, we then present simulations on a platform based on molecular spin qudits [22, 27, 72], which allows for a hardware-efficient implementation of our scheme. Numerical simulations of all the QEC gadgets show that the logical error after correction propagates to higher orders than the physical error affecting the system (i.e. the error is suppressed to a larger extent). This demonstrates FTQC. Moreover, we find that logical errors decrease almost exponentially with the number of levels in the encoding.

General protocol – We first introduce the general mathematical framework of the stabilizer codes and then show which properties are needed on the hardware for their FT implementation.

Errors corrupting quantum information initially encoded in the pure state $\rho_0 = |\psi_0\rangle \langle \psi_0|$ are represented by Kraus operators E_k , i.e. the density matrix after possible errors is $\rho = \sum_k E_k \rho_0 E_k^{\dagger}$. Protection against a set of errors $\{E_k\}$ can be achieved by identifying code words $|0_L\rangle$ and $|1_L\rangle$ which satisfy Knill-Laflamme conditions [36]:

$$\langle 0_L | E_k^{\dagger} E_j | 0_L \rangle = \langle 1_L | E_k^{\dagger} E_j | 1_L \rangle$$
 (1a)

$$\langle 0_L | E_k^{\dagger} E_j | 1_L \rangle = 0. \tag{1b}$$

By using d dimensional qudits, at most d/2 different errors can be corrected. We then consider the vector set $\{|0_L\rangle, E_k|0_L\rangle, |1_L\rangle, E_k|1_L\rangle\}_{k=1}^{d/2}$, and the orthonormal basis set \mathcal{A} obtained from its Gram-Schmidt orthogonalization. We denote the set \mathcal{A} of error words as $\{|\ell,k\rangle\}$ with $\ell=0,1$ and $k=0,\ldots,d/2$.

This choice highlights the basic idea to achieve FTQC, to perform logical operations independently of the error k [37]. Formally, given a gate G on a single qubit, the corresponding logical gate G_L that extends G to the protected LQ is given by $G_L \doteq G \otimes I_{d/2}$. This is equivalent to defining the logical Pauli operators:

$$X_L = \sum_{k=0}^{d/2-1} (|0,k\rangle \langle 1,k| + |1,k\rangle \langle 0,k|)$$
 (2a)

$$Z_L = \sum_{k=0}^{d/2-1} (|0,k\rangle \langle 0,k| - |1,k\rangle \langle 1,k|)$$
 (2b)

and $Y_L = -iZ_LX_L$. Then, a generic logical rotation about $\sigma = X, Y, Z$ is obtained $R_L^{\sigma}(\theta) = \exp[-i\sigma_L\theta/2]$. Two-qubit controlled logical gates CG can be realized in a similar way, by implementing CG independently of the error k on both the (logical) control and target (see SM). Finally, readout of the state of the LQ corresponds to a measurement of Z_L , which again translates into distinguishing the value of ℓ independently of the error k. Error detection translates into the stabilization of information through the measurement of

$$S = \sum_{k,\ell} \lambda_k |\ell, k\rangle \langle \ell, k| \tag{3}$$

where $\lambda_k \neq \lambda_{k'}$ for $k \neq k'$. This is the extension of stabilizers codes on qubits, with the important simplification that we have only one multi-valued stabilizer that gives directly the error syndrome instead of multiple twovalued stabilizers [38, 39]. This reduces the impact of measurement errors (see below). Stabilization is achieved by exploiting a d/2-levels ancilla linked to the d-levels LQ and implementing a k-controlled operation CU [Fig. 1-(b)] between the logical qubit (control, initially in a generic state $|\bar{\psi}\rangle$) and the ancilla (target, initialized in its ground state $|0\rangle$). The action of the CU gate is defined as: $|\ell, k\rangle |0\rangle \mapsto |\ell, k\rangle |k\rangle$, $|\ell, k\rangle |k\rangle \mapsto -|\ell, k\rangle |0\rangle$ and the identity otherwise [40]. Therefore, CU maps each error kto a specific eigenstate of the ancilla. Hence, a final measurement of the ancilla in its eigenbasis $[M_z \text{ in Fig. 1-(b)}]$ identifies the error syndrome k and stabilizes information in the subspace $|\ell, k\rangle$. The final recovery step R_k consists in mapping the stabilized $|\ell, k \neq 0\rangle$ into $|\ell, k = 0\rangle$.

Implementation – The actual FT implementation of the QC gadgets (EC, one- and two-qubit gates, readout) requires to perform them directly on encoded states, avoiding any decoding step [7]. We show this can be achieved by assuming a LQ encoded in a d-level quantum system in which transitions between any pair of levels can be induced by external stimuli (all-to-all connectivity).

As a prototypical example, we consider spin gudits encoded in Molecular Nanomagnets (MNMs), i.e clusters containing few interacting spins, whose spin Hamiltonian is usually well characterized and can be tailored to fit specific requirements [27, 41–45]. In particular, multispin molecules characterized by a proper pattern of antiferromagnetic competing exchange interactions display many low-energy multiplets with an all-to-all connectivity thanks to anisotropies [71, 72]. Hence, MNMs naturally provide a hardware-efficient implementation of the abstract concepts introduced above. In these systems (as in trapped ions [47, 48], atoms [49] and several other spin architectures [50, 51]) pure dephasing is by far the leading error (with decay time T_2), while spin relaxation at low temperature is orders of magnitude slower [52–54]. Therefore, we focus on pure dephasing.

Fig. 2 illustrates the implementation of representative single-qubit gadgets, focusing for simplicity on a 4-levels LQ. The extension to larger qudits is straightforward. Hereafter we use the error words derived in Ref. [72] for a molecular multi-spin cluster interacting with a nuclear spin bath which drives decoherence, because the specific choice does not qualitatively affect our conclusions. Let's start from a logical planar rotation $R_L^P(\theta,\phi) = \exp\left[-i\left(\cos\phi\,Y_L - \sin\phi\,X_L\right)\theta/2\right]$. From (2),

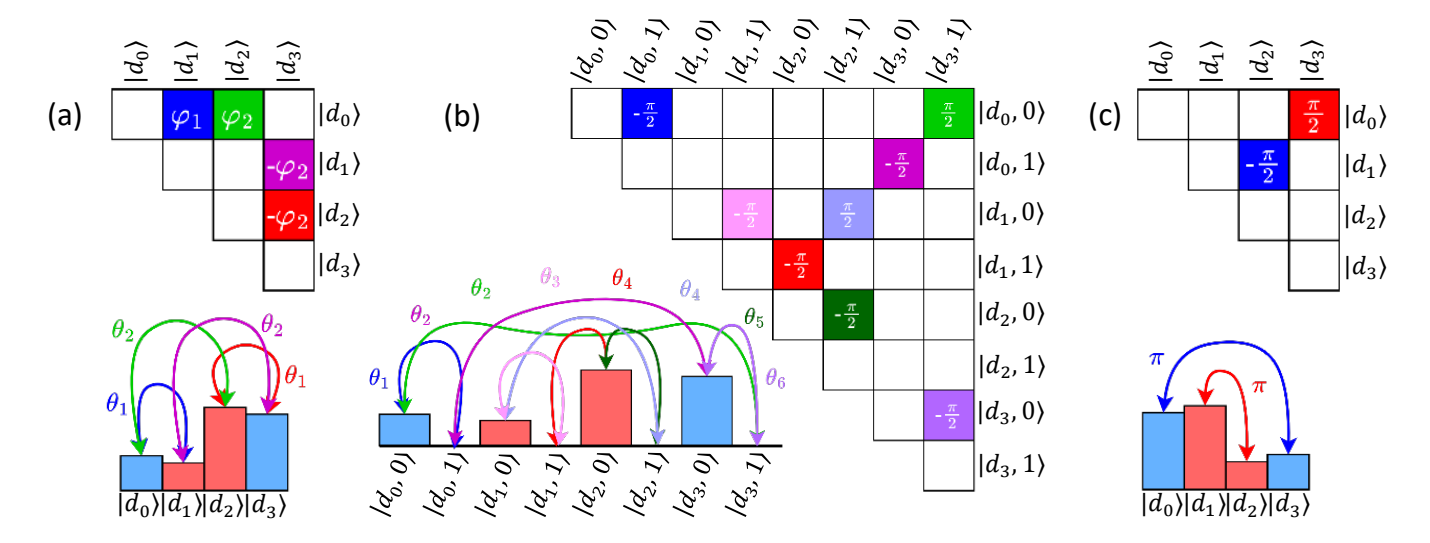


Figure 2: Scheme of single-qubit gates (a), stabilization (b), and recovery (c) for a d=4 LQ, using the code words derived in Ref. [72]. In each panel the left histogram represents the populations of the eigenstates $(|d_j\rangle)$ assuming $\alpha=\beta=1/\sqrt{2}$, in blue (orange) for $\ell=0(1)$. The upper triangular matrix on the right is the driving Hamiltonian in the rotating frame, with filled boxes indicating the set of θ_i resonant pulses between pairs of eigenstates (arrows in the histograms) which are simultaneously sent to the system. Different colors of the arrows and boxes indicate different pulse frequencies, while phases are indicated on top. Eigenstates of the system qudit are indicated as $|d_j\rangle$, j=0,...,3. For stabilization (b) the eigenstates of a two-level ancilla (0,1) are also reported.

we note that its realization requires resonant pulses between each eigenstate in the logical $\ell=0$ subspace [blue bars in Fig. 2-(a)] and each one in the logical $\ell=1$ subspace (orange bars). Different pulses of length θ_j are indicated by double arrows in the histogram and their phase φ_j is reported in the connectivity matrix \tilde{H} nearby. As detailed in the SM, one can show (with a generalized rotating frame formalism [55]) that the set of simultaneous pulses $\{\theta_j,\varphi_j\}$ implements the unitary $\exp\left[-i\tilde{H}\right]$, which corresponds to $R_L^P(\theta,\phi)$. Here we assume all the energy gaps to be spectroscopically distinguishable. Remarkably, since $\theta,\phi\in\mathbb{R}$, the resulting set of gates $R_L^P(\theta,\phi)$ is a universal set for a single logical qubit.

We now examine the stabilization process, reported in Fig. 2-(b). In this case, the eigenstates of both the LQ and of a d/2 levels ancilla are shown in the product basis $|d_i, k\rangle$. We recall that the ancilla is initialized in its ground state $|0\rangle$. CU stabilization requires to excite the ancilla iff the LQ is in k=1. This translates into the set of simultaneous pulses indicated in Fig. 2-(b) between each qudit eigenstate $|d_i\rangle$ with the ancilla in $|0\rangle$ and each qudit eigenstate $|d_i\rangle$ with the ancilla in $|1\rangle$. Following the argument above, one can derive the connectivity matrix with pulse lengths and phases by taking the logarithm of CU (see SM). It is important to note that the ancilla does not need to be encoded. Indeed, it is excited to the eigenstate $|k\rangle$ with the same probability p_k of having an error E_k . Then, it suffers an error $E_{k'}$ with the conditional probability $p_k p_{k'}$ which therefore results to be of a higher order than the error on the qudit.

Fig. 2-(c) also shows the recovery step from k=1 to k=0, which is obtained by a pair of pulses within the two disjoint $\ell=0,1$ subspaces [56]. Other single-qubit gadgets (e.g., encoding) can be analogously obtained. Final k-independent readout of the LQ is accomplished by distinguishing orange and blue bars in the histograms of Fig. 2. Notice that fault-tolerance of all these operations is ensured by the all-to-all connectivity, which enables us to never decode the LQ and hence not to introduce additional errors.

Simulations - We now demonstrate the effectiveness of the single-qubit gadgets described above by numerical simulations in which we integrate the Lindblad equation for the system density matrix, subject both to pure dephasing and to the required sequence of pulses (see SM). In particular, we consider generic $R_L^P(\theta,\phi)$ rotations, followed by stabilization and correction and we report [Fig. 3-(a)] the final logical error $\bar{\mathcal{E}}_e$ as a function of the elementary error rate $1/T_2$. Here $\mathcal{E}_e = 1 - \mathcal{F}_e^2$, where \mathcal{F}_e is the entanglement fidelity [20] of the procedure [57], and we average on a universal set of (θ, ϕ) values. The logical error is obtained by full state tomography of the logical state and corresponds to the failure probability of the EC procedure, i.e. to errors which cannot be corrected by the code. We immediately note that the slope of the curves in Fig. 3-(a) in log-log scale for the encoded LQ (number of levels ≥ 4) is larger than for the uncorrected case (blue line). This means that $\bar{\mathcal{E}}_e$ is propagated through the gadgets of the executed circuit to a higher order than the elementary error, thus demonstrating the Fault Tolerance of all the procedures involved. Notably,

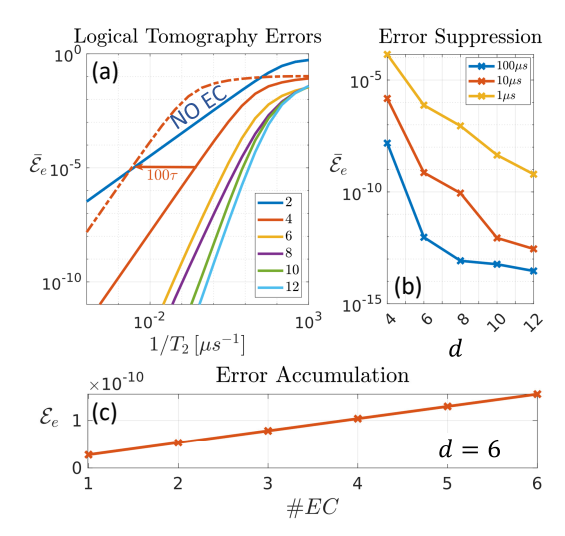


Figure 3: Simulation of the FTqd implementation of single qubit logical gates on a MNM [72]. (a) Error $\mathcal{E}_e = 1 - \mathcal{F}_e^2$ as a function of $1/T_2$, where \mathcal{F}_e is the entanglement fidelity [20], averaged over different planar rotations $R_L^p(\theta,\varphi)$ for $(\theta,\phi) = (\frac{\pi}{4},\pi), (\frac{\pi}{2},\pi), (\frac{\pi}{2},-\frac{\pi}{2}), (\frac{\pi}{2},-\frac{\pi}{4}), (\frac{\pi}{2},-\frac{\pi}{8})$. (b) Performance of the code as function of the number of levels for different values of T_2 . (c) Accumulation of the error as a function of the number of "Logical Gate-Error Correction" cycles, for 6 qudit levels and $T_2 = 50 \ \mu s$, showing a linear trend as required for FT.

for reasonable duration of the pulses [58–60] this holds independently of T_2 , i.e. there is no threshold.

Leakage errors could arise due to the finite duration of the pulses, but can be largely reduced by pulse-shaping techniques [61] and/or by using long pulses. Indeed, Figure 3-(a) shows that τ can be largely increased without compromising FT. For instance, by increasing τ by a factor 100 (dashed orange line), the slope of the curve for $T_2 \gtrsim 100~\mu s$ (still reasonable for several MNMs [62, 63]) does not change and hence the error is still propagated to a higher order compared to the uncorrected qubit. We only get a threshold in the minimal required T_2 .

Moreover, by increasing the LQ size d the error is further reduced and propagated to an even higher order, as evidenced by the increase of the slope of the curves in Fig. 3-(a). Remarkably, we find an almost exponential suppression of the error with a linear increase of d, as reported in Fig. 3-(b), independently of T_2 . The final error suppression is strikingly large when compared to standard multi-qubit codes: here we achieve a logical error of 10^{-12} by employing 12×6 levels (LQ+ancilla) and $T_2 = 10 \ \mu s$, which should be compared to more than 5000 qubits needed by Floquet or surface codes with the same elementary error $p \approx \tau/T_2 = 3/1000$ [19]. This remarkable performance, obtained exploiting qudits with all-to-all connectivity, is here shown by focusing on the dominant family of errors of molecular qudits. The appli-

cation of FTqd to other errors requires to identify suitable code words and will be focus of a future work. Moreover, the depth of our circuit does not increase with d, since all operations are implemented in parallel, again in contrast with standard codes. Remarkably, here a single measurement is sufficient for the syndrome and the corresponding error [64] can be suppressed by repeated measures as shown by simulations in the SM. Finally, Fig. 3-(c) shows the accumulation of the logical error after a sequence of gate-EC cycles. The perfectly linear trend shows that the procedure does not introduce any additional uncorrectable error, i.e. it is FT.

We now consider a two-qubit logical gate, such as the controlled-phase $C-\varphi$. This can be implemented by considering three interacting LQs, where the middle one acts as a switch of the effective coupling between the other two [65, 66], Q_1 and Q_2 (inset of Fig. 4). In presence of an interaction between the three units, excitations of the switch are dependent on the state of both Q_1 and Q_2 . This allows us to induce a 2π (semi-)resonant excitation of the switch (initialized in $|\bar{0}\rangle$) only for a specific $|\psi_1\psi_2\rangle$ logical state, such as $|\bar{1}1\rangle$. As a result, a phase is added only to the $|\bar{11}\rangle$ component of the two-qubit logical state [65–68], i.e. a $C-\varphi$ gate is implemented (see also SM). Since this involves a logical rotation $R_L^P(2\pi,0)$ of the switch, the latter must also be encoded and corrected. Simulation of the two-qubit gate followed by EC on all the three units is shown in Fig. 4 for d = 4. As for single-qubit gates, the logical error is suppressed (here for $T_2 \gtrsim 30 \ \mu s$), thus demonstrating FTQC on a univer-

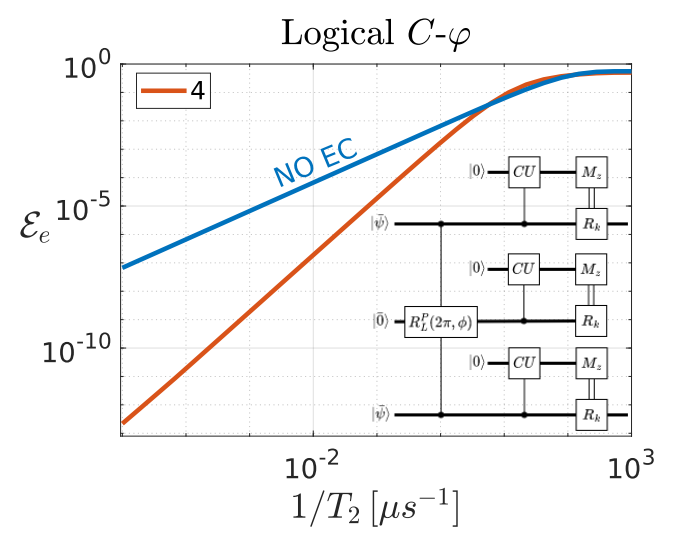


Figure 4: Numerical simulation of the FT implementation of two-qubit logical gates. The uncorrectable logical error is shown as a function of $1/T_2$ at the end of a "Logical C- φ - EC" cycle. Simulations are computationally demanding and hence we limit to d=4. Inset: simulated circuit, with two logical qubits $|\bar{\psi}\rangle$ in a generic state, coupled by an error-corrected switch initialized in $|0_L\rangle$. Each unit is coupled to a d/2-levels ancilla for stabilization.

sal set of gates.

The scheme can be implemented also with simpler systems at the cost of reduced performance. For instance, single-spin molecules in presence of transverse magnetic fields and/or high-rank zero-field splitting anisotropy provide the all-to-all connectivity required by FTqd. Moreover, the scheme could be adapted to other multilevel quantum systems like impurity nuclear spins in semiconductor [51], atoms [69] or ion traps [48].

Conclusions – We have introduced a scheme for Fault-Tolerant quantum computing where each elementary logical qubit is encoded into a single multi-level qudit. The scheme only relies on an all-to-all connectivity between the state entering the definition of the logical qubit. The remarkable performance of the code is demonstrated by considering its implementation on a molecular spin architecture [68]. Our approach prevents the blowing up in the number of physical units, while yielding a large error suppression already with a small number of qudit levels, thus making the pro-

posed route very appealing for an actual implementation.

[†]These Authors contributed equally to the work.

ACKNOWLEDGMENTS

We warmly thank P. Santini for useful and stimulating discussions.

This work received financial support from European Union – NextGenerationEU, PNRR MUR project PE0000023-NQSTI, from the European Union's Horizon 2020 program under Grant Agreement No. 862893 (FET-OPEN project FATMOLS) and from Fondazione Cariparma. Project funded by the European Union – NextGenerationEU under the National Recovery and Resilience Plan (NRRP), Mission 4 Component 1 Investment 3.4 and 4.1. Decree by the Italian Ministry n. 351/2022 CUP D92B22000530005.

- [1] R. Chao and B. W. Reichardt, Fault-tolerant quantum computation with few qubits, npj Quantum Inf. 4, 42 (2018).
- [2] D. Gottesman, An introduction to quantum error correction (2000), arXiv:quant-ph/0004072 [quant-ph].
- [3] S. J. Devitt, W. J. Munro, and K. Nemoto, Quantum error correction for beginners, Rep. Progr. Phys. 76, 076001 (2013).
- [4] D. Nigg, M. Müller, E. A. Martinez, P. Schindler, M. Hennrich, T. Monz, M. A. Martin-Delgado, and R. Blatt, Quantum computations on a topologically encoded qubit, Science 345, 302 (2014).
- [5] B. M. Terhal, Quantum error correction for quantum memories, Rev. Mod. Phys. 87, 307 (2015).
- [6] E. Campbell, B. Terhal, and C. Vuillot, Roads towards fault-tolerant universal quantum computation, Nature 549, 172 (2017).
- [7] M. A. Nielsen and I. L. Chuang, Quantum Computation and Quantum Information (Cambridge university press, 2000).
- [8] P. Aliferis, D. Gottesman, and J. Preskill, Quantum accuracy threshold for concatenated distance-3 codes, Quant. Inf. Comput. 6, 97–165 (2006).
- [9] E. Knill, Quantum computing with realistically noisy devices, Nature 434, 39 (2005).
- [10] A. W. Cross, D. P. Divincenzo, and B. M. Terhal, A comparative code study for quantum fault tolerance, Quantum Info. Comput. 9, 541–572 (2009).
- [11] D. S. Wang, A. G. Fowler, and L. C. L. Hollenberg, Surface code quantum computing with error rates over 1%, Phys. Rev. A 83, 020302 (2011).
- [12] A. G. Fowler, A. M. Stephens, and P. Groszkowski, Highthreshold universal quantum computation on the surface code, Phys. Rev. A 80, 052312 (2009).
- [83] A. G. Fowler, M. Mariantoni, J. M. Martinis, and A. N. Cleland, Surface codes: Towards practical large-scale quantum computation, Phys. Rev. A 86, 032324 (2012).

- [14] A. M. Stephens, Fault-tolerant thresholds for quantum error correction with the surface code, Phys. Rev. A 89, 022321 (2014).
- [15] C. Chamberland, T. Jochym-O'Connor, and R. Laflamme, Thresholds for universal concatenated quantum codes, Phys. Rev. Lett. 117, 010501 (2016).
- [16] J. Marks, T. Jochym-O'Connor, and V. Gheorghiu, Comparison of memory thresholds for planar qudit geometries, New J. Phys. 19, 113022 (2017).
- [17] E. T. Campbell, Enhanced fault-tolerant quantum computing in d-level systems, Phys. Rev. Lett. 113, 230501 (2014).
- [18] M. Suchara, J. Kubiatowicz, A. Faruque, F. T. Chong, C.-Y. Lai, and G. Paz, Qure: The quantum resource estimator toolbox, in 2013 IEEE 31st International Conference on Computer Design (ICCD) (2013) pp. 419–426.
- [19] A. Paetznick, C. Knapp, N. Delfosse, B. Bauer, J. Haah, M. B. Hastings, and M. P. da Silva, Performance of planar floquet codes with majorana-based qubits, PRX Quantum 4, 010310 (2023).
- [20] E. Knill, R. Laflamme, R. Martinez, and C. Negrevergne, Benchmarking quantum computers: The five-qubit error correcting code, Phys. Rev. Lett. 86, 5811 (2001).
- [21] S. Pirandola, S. Mancini, S. L. Braunstein, and D. Vitali, Minimal qudit code for a qubit in the phase-damping channel, Phys. Rev. A 77, 032309 (2008).
- [22] A. Chiesa, E. Macaluso, F. Petiziol, S. Wimberger, P. Santini, and S. Carretta, Molecular nanomagnets as qubits with embedded quantum-error correction, J. Phys. Chem. Lett. 11, 8610 (2020).
- [23] M. H. Michael, M. Silveri, R. Brierley, V. V. Albert, J. Salmilehto, L. Jiang, and S. M. Girvin, New class of quantum error-correcting codes for a bosonic mode, Phys. Rev. X 6, 031006 (2016).
- [24] W. Cai, Y. Ma, W. Wang, C.-L. Zou, and L. Sun, Bosonic quantum error correction codes in superconducting quantum circuits, Fundamental Research 1, 50 (2021).

- [25] S. Omanakuttan and J. A. Gross, Multispin clifford codes for angular momentum errors in spin systems (2023), arXiv:2304.08611 [quant-ph].
- [26] F. Petiziol, A. Chiesa, S. Wimberger, P. Santini, and S. Carretta, Counteracting dephasing in molecular nanomagnets by optimized qudit encodings, npj Quantum Inf. 7, 133 (2021).
- [27] S. Carretta, D. Zueco, A. Chiesa, A. Gómez-León, and F. Luis, A perspective on scaling up quantum computation with molecular spins, Appl. Phys. Lett. 118, 240501 (2021).
- [28] M. Chizzini, L. Crippa, L. Zaccardi, E. Macaluso, S. Carretta, A. Chiesa, and P. Santini, Quantum error correction with molecular spin qudits, Phys. Chem. Chem. Phys. 24, 20030 (2022).
- [29] S. Lim, J. Liu, and A. Ardavan, Fault-tolerant qubit encoding using a spin-7/2 qudit (2023), arXiv:2303.02084 [quant-ph].
- [30] Z. Ni, S. Li, X. Deng, Y. Cai, L. Zhang, W. Wang, Z.-B. Yang, H. Yu, F. Yan, S. Liu, C.-L. Zou, L. Sun, S.-B. Zheng, Y. Xu, and D. Yu, Beating the break-even point with a discrete-variable-encoded logical qubit, Nature 616, 56 (2023).
- [31] P. Reinhold, S. Rosenblum, W.-L. Ma, L. Frunzio, L. Jiang, and R. J. Schoelkopf, Error-corrected gates on an encoded qubit, Nat. Phys. 16, 822 (2020).
- [32] S. Puri, L. St-Jean, J. A. Gross, A. Grimm, N. E. Frattini, P. S. Iyer, A. Krishna, S. Touzard, L. Jiang, A. Blais, S. T. Flammia, and S. M. Girvin, Bias-preserving gates with stabilized cat qubits, Sci. Adv. 6, eaay5901 (2020).
- [33] S. Rosenblum, P. Reinhold, M. Mirrahimi, L. Jiang, L. Frunzio, and R. J. Schoelkopf, Fault-tolerant detection of a quantum error, Science 361, 266 (2018).
- [34] L. Hu, Y. Ma, W. Cai, X. Mu, Y. Xua, W. Wang, Y. Wu, H. Wang, Y. P. Song, C.-L. Zou, S. M. Girvin, L.-M. Duan, and L. Sun, Quantum error correction and universal gate set operation on a binomial bosonic logical qubit, Nat. Phys. 15, 503–508 (2019).
- [72] A. Chiesa, F. Petiziol, M. Chizzini, P. Santini, and S. Carretta, Theoretical design of optimal molecular qudits for quantum error correction, J. Phys. Chem. Lett. 13, 6468 (2022).
- [36] E. Knill and R. Laflamme, Theory of quantum errorcorrecting codes, Phys. Rev. A 55, 900 (1997).
- [37] Y. Ma, Y. Xu, X. Mu, W. Cai, L. Hu, W. Wang, X. Pan, H. Wang, Y. P. Song, C.-L. Zou, and L. Sun, Errortransparent operations on a logical qubit protected by quantum error correction, Nat. Phys. 16, 827–831 (2020).
- [38] A. G. Fowler, A. C. Whiteside, and L. C. L. Hollenberg, Towards practical classical processing for the surface code, Phys. Rev. Lett. 108, 180501 (2012).
- [39] S. Bravyi, M. Suchara, and A. Vargo, Efficient algorithms for maximum likelihood decoding in the surface code, Phys. Rev. A 90, 032326 (2014).
- [40] The relative phase between $|\ell,k\rangle|0\rangle$ and $|\ell,k\rangle|k\rangle$ is necessary to ensure that the corresponding Hamiltonian has zero diagonal. Since the ancilla is initialized in $|0\rangle$, this relative phase is irrelevant.
- [41] D. Gatteschi, R. Sessoli, and J. Villain, Molecular Nanomagnets (Oxford University Press, 2006).
- [42] M. Shiddiq, D. Komijani, Y. Duan, A. Gaita-Ariño, E. Coronado, and S. Hill, Enhancing coherence in molecular spin qubits via atomic clock transitions., Nature 531, 348 (2016).

- [43] F. Troiani and M. G. A. Paris, Universal quantum magnetometry with spin states at equilibrium, Phys. Rev. Lett. 120, 260503 (2018).
- [44] A. Gaita-Ariño, F. Luis, S. Hill, and E. Coronado, Molecular spins for quantum computation., Nat. Chem. 11, 301 (2019).
- [45] M. Atzori and R. Sessoli, The second quantum revolution: Role and challenges of molecular chemistry, J. Am. Chem. Soc. 141, 11339 (2019).
- [71] M. Chizzini, L. Crippa, A. Chiesa, F. Tacchino, F. Petiziol, I. Tavernelli, P. Santini, and S. Carretta, Molecular nanomagnets with competing interactions as optimal units for qudit-based quantum computation, Phys. Rev. Res. 4, 043135 (2022).
- [47] C. D. Bruzewicz, J. Chiaverini, R. McConnell, and J. M. Sage, Trapped-ion quantum computing: Progress and challenges, Appl. Phys. Lett. 6, 021314 (2019).
- [48] M. Ringbauer, M. Meth, L. Postler, R. Stricker, R. Blatt, P. Schindler, and T. Monz, A universal qudit quantum processor with trapped ions, Nat. Phys. 18, 1053–1057 (2022).
- [49] S. Kuhr, W. Alt, D. Schrader, I. Dotsenko, Y. Miroshnychenko, A. Rauschenbeutel, and D. Meschede, Analysis of dephasing mechanisms in a standing-wave dipole trap, Phys. Rev. A 72, 023406 (2005).
- [50] A. Morello, J. J. Pla, P. Bertet, and D. N. Jamieson, Donor spins in silicon for quantum technologies, Adv. Quantum Technol. 3, 2000005 (2020).
- [51] A. Chatterjee, P. Stevenson, S. De Franceschi, A. Morello, N. P. de Leon, and F. Kuemmeth, Semiconductor qubits in practice, Nat. Rev. Phys. 3, 157 (2021).
- [52] M. Fataftah, J. M. Zadrozny, S. C. Coste, M. J. Graham, D. M. Rogers, and D. E. Freedman, Employing forbidden transitions as qubits in a nuclear spin-free chromium complex., J. Am. Chem. Soc. 138, 1344 (2016).
- [53] K. Bader, M. Winkler, and J. van Slageren, Tuning of molecular qubits: Very long coherence and spin–lattice relaxation times, Chem. Commun., 3623 (2016).
- [54] Y.-S. Ding, Y.-F. Deng, and Y.-Z. Zheng, The rise of single-ion magnets as spin qubits, Magnetochem. 2, 40 (2016).
- [55] M. N. Leuenberger and D. Loss, Grover algorithm for large nuclear spins in semiconductors, Phys. Rev. B 68, 165317 (2003).
- [56] This is due to the specific form of the error words $\{|\ell,k\rangle\}$, in which differ the two $\ell=0,1$ subspaces are disjoint for all k.
- [57] \mathcal{F}_e is the average fidelity on the initial states $|0_L\rangle$, $|1_L\rangle$, $\frac{1}{\sqrt{2}}(|0\rangle + |1\rangle)$, $\frac{1}{\sqrt{2}}(|0\rangle |1\rangle)$, $\frac{1}{\sqrt{2}}(|0\rangle + i|1\rangle)$, $\frac{1}{\sqrt{2}}(|0\rangle i|1\rangle)$.
- [58] M. Atzori, E. Morra, L. Tesi, A. Albino, M. Chiesa, L. Sorace, and R. Sessoli, Quantum coherence times enhancement in vanadium(iv)-based potential molecular qubits: the key role of the vanadyl moiety, J. Am. Chem. Soc. 138, 11234 (2016).
- [59] M. Atzori, L. Tesi, E. Morra, M. Chiesa, L. Sorace, and R. Sessoli, Room-temperature quantum coherence and rabi oscillations in vanadyl phthalocyanine: Toward multifunctional molecular spin qubits., J. Am. Chem. Soc. 138, 2154 (2016).
- [60] M. Atzori, E. Garlatti, G. Allodi, S. Chicco, A. Chiesa, A. Albino, R. D. Renzi, E. Salvadori, M. Chiesa, S. Carretta, and L. Sorace, Radiofrequency to microwave coherent manipulation of an organometallic electronic spin

- qubit coupled to a nuclear qudit, Inorganic Chemistry **60**, 11273 (2021).
- [61] A. Castro, A. García Carrizo, S. Roca, D. Zueco, and F. Luis, Optimal control of molecular spin qudits, Phys. Rev. Appl. 17, 064028 (2022).
- [62] K. Bader, D. Dengler, S. Lenz, B. Endeward, S.-D. Jiang, P. Neugebauer, and J. van Slageren, Room temperature quantum coherence in a potential molecular qubit, Nat. Comm. 5, 5304 (2014).
- [63] J. M. Zadrozny, J. Niklas, O. G. Poluektov, and D. E. Freedman, Millisecond coherence time in a tunable molecular electronic spin qubit., ACS Cent. Sci. 1, 488 (2015).
- [64] A. Kandala, A. Mezzacapo, K. Temme, M. Takita, M. Brink, J. M. Chow, and J. M. Gambetta, Hardwareefficient variational quantum eigensolver for small molecules and quantum magnets, Nature 549, 242–246 (2017).
- [65] J. Ferrando-Soria, E. Moreno-Pineda, A. Chiesa, A. Fernandez, S. A. Magee, S. Carretta, P. Santini, I. Vitorica-Yrezabal, F. Tuna, E. J. L. McInness, and R. E. P. Winpenny, A modular design of molecular qubits to implement universal quantum gates., Nat. Commun. 7, 11377 (2016).
- [66] A. Chiesa, F. Petiziol, E. Macaluso, S. Wimberger, P. Santini, and S. Carretta, Embedded quantum-error correction and controlled-phase gate for molecular spin qubits, AIP Adv. 11, 025134 (2021).
- [67] A. Chiesa, G. F. S. Whitehead, S. Carretta, L. Carthy, G. A. Timco, S. J. Teat, G. Amoretti, E. Pavarini, R. E. P. Winpenny, and P. Santini, Molecular nanomagnets with switchable coupling for quantum simulation., Sci. Rep. 4, 7423 (2014).
- [68] A. Chiesa, S. Roca, S. Chicco, M. de Ory, A. Gómez-León, A. Gomez, D. Zueco, F. Luis, and S. Carretta, Blueprint for a molecular-spin quantum processor, Phys. Rev. Appl. 19, 064060 (2023).
- [69] A. V. Gorshkov, M. Hermele, V. Gurarie, C. Xu, P. S. Julienne, J. Ye, P. Zoller, E. Demler, M. D. Lukin, and A. M. Rey, Two-orbital s u(n) magnetism with ultracold alkaline-earth atoms, Nat. Phys. 6, 289 (2010)

- [70] G. K. Brennen, D. P. O'Leary, and S. S. Bullock, Phys. Rev. A 71, 052318 (2005).
- [71] M. Chizzini, L. Crippa, A. Chiesa, F. Tacchino, F. Petiziol, I. Tavernelli, P. Santini, and S. Carretta, Phys. Rev. Res. 4, 043135 (2022).
- [72] A. Chiesa, F. Petiziol, M. Chizzini, P. Santini, and S. Carretta, J. Phys. Chem. Lett. 13, 6468 (2022).
- [73] A. Chiesa, P. Santini, D. Gerace, J. Raftery, A. A. Houck, and S. Carretta, Sci. Rep. 5, 16036 (2015).
- [74] E. Garlatti, S. Carretta, M. Affronte, E. C. Sañudo, G. Amoretti, and P. Santini, J. Phys.: Cond. Matt. 24, 104006 (2012).
- [75] M. Antkowiak, P. Kozłowski, G. Kamieniarz, G. A. Timco, F. Tuna, and R. E. P. Winpenny, Phys. Rev. B 87, 184430 (2013).
- [76] M. Baker, G. Timco, S. Piligkos, J. Mathieson, H. Mutka, F. Tuna, P. Kozlowski, M. Antkowiak, T. Guidi, T. Gupta, H. Rath, R. Woolfson, G. Kamieniarz, R. Pritchard, H. Weihe, L. Cronin, G. Rajaraman, D. Collison, E. McInnes, and R. Winpenny, Proc. Natl. Acad. Sci. U.S.A. 109, 19113 (2012).
- [77] W. Florek, M. Antkowiak, and G. Kamieniarz, Phys. Rev. B 94, 224421 (2016).
- [78] Y. Furukawa, K. Kiuchi, K.-i. Kumagai, Y. Ajiro, Y. Narumi, M. Iwaki, K. Kindo, A. Bianchi, S. Carretta, P. Santini, F. Borsa, G. A. Timco, and R. E. P. Winpenny, Phys. Rev. B 79, 134416 (2009).
- [79] L. M. Baker and et al., Chem. A Eur. J. 22, 1779 (2016).
- [80] R. J. Woolfson, G. A. Timco, A. Chiesa, I. J. Vitorica-Yrezabal, F. Tuna, T. Guidi, E. Pavarini, P. Santini, S. Carretta, and R. E. P. Winpenny, Angew. Chem. Int. Ed. 55, 8856 (2016).
- [81] K. Blum, Density Matrix Theory and Applications (Springer Berlin Heidelberg, 2012)A. Kandala, A. Mezzacapo, K. Temme, M. Takita, M. Brink, J. M. Chow, and J. M. Gambetta, Nature 549, 242–246 (2017).
- [82] S. Barnett, Quantum information, Vol. 16 (Oxford University Press, 2009).
- [83] A. G. Fowler, M. Mariantoni, J. M. Martinis, and A. N. Cleland, Phys. Rev. A 86, 032324 (2012).

Appendix A: Derivation of the pulse sequence

We now show how to derive the sequence of pulses to implement the various quantum computing operations (a.k.a. gadgets) described in the main text. The all-to-all connectivity we consider implies that it is possible to drive transitions between any pair of qudit levels by a pulse resonant with the energy gap between the two states. In addition, all pulses are assumed to be spectroscopically distinguishable, as reasonable for Molecular Nanomagnets, possibly with the help of suitable pulse-shaping techniques [61].

With these hypotheses and working in the basis of the eigenstates of the static system Hamiltonian $H_0 = \sum_{j=0}^{d-1} E_j |d_j\rangle \langle d_j|$, a set of simultaneous (circularly polarized) transverse pulses each addressing a different transition between a pair of qudit eigenstates can be described by the time-dependent Hamiltonian ($\hbar = 1$):

$$H_1(t) = \sum_{i < j} b_{ij} m_{ij} e^{-i(\omega_{ij}t + \phi_{ij})} |d_i\rangle \langle d_j| + \text{h.c.}.$$
(A1)

Note that each amplitude b_{ij} , frequency ω_{ij} and phase ϕ_{ij} can be controlled independently, while m_{ij} is the system-dependent matrix element between the two eigenstates $|d_i\rangle$ and $|d_j\rangle$. Assuming, without loss of generality, axial symmetry in H_0 , we get $m_{ij} = \langle d_i | M_x | d_j \rangle$, where M_x is the dipole magnetic moment orthogonal to the quantization axis. This driving Hamiltonian can be made time independent by moving to a generalized rotating frame [55], via the

unitary transformation

$$U_{\text{rot}} = \sum_{j} e^{i\,\omega_{0j}t} |d_{j}\rangle \langle d_{j}| \tag{A2}$$

where $\omega_{0,k} = \sum_{j=1}^k \omega_{j-1,j}$. This leads to the generalized rotating frame Hamiltonian $H_{\text{rot}} = U_{\text{rot}}[H_1(t) + H_0]U_{\text{rot}}^{\dagger} - iU_{\text{rot}}\dot{U}_{\text{rot}}^{\dagger}$. H_{rot} takes the form:

$$H_{\text{rot}} = \sum_{i < j} \theta_{ij} e^{-i\varphi_{ij}} |d_i\rangle \langle d_j| + \text{h.c.} + \sum_{j=1}^{d-1} (E_j - \omega_{0j}) |d_j\rangle \langle d_j|$$
(A3)

where $\theta_{ij} = b_{ij} m_{ij}$ and we have set $E_0 = 0$. The resulting time evolution can be computed in the generalized rotating frame as $e^{-iH_{\rm rot}t}$. This shows that by choosing the set of ω_{ij} to be in resonance with the energy gaps in H_0 we selectively activate transitions between given pairs of eigenstates, while other states which are significantly off-resonance are not affected.

Note that in practice this corresponds to the time evolution induced by an effective Hamiltonian \tilde{H} with zero diagonal and only some of the off diagonal terms activated at will, depending on the gadget that we aim to implement. This procedure can be realized in one shot with a single multi-frequency pulse and is the key to ensure Fault Tolerance. Below we show that each gadget can indeed be decomposed along these lines and recast into an effective zero-diagonal Hamiltonian \tilde{H} , corresponding to the different panels of Fig. 2 in the main text. Possible presence of diagonal terms in \tilde{H} would require a slightly more complex pulse sequence.

Appendix B: Fault-tolerant logical single-qubit rotations

We now describe a universal set of logical gates. First we recall that any unitary gate on a qudit can be decomposed (up to a global phase) into planar rotations (PRs) among any pair of levels [68, 70, 71], i.e.

$$R_{ij}^{P}(\theta,\varphi) \doteq \cos\frac{\theta}{2} \left(|d_i\rangle \langle d_i| + |d_j\rangle \langle d_j| \right) + \sin\frac{\theta}{2} \left(-e^{-i\varphi} |d_i\rangle \langle d_j| + e^{i\varphi} |d_j\rangle \langle d_i| \right). \tag{B1}$$

Each PR can be implemented by a pulse resonant with the energy gap $E_j - E_i$, as discussed above. Indeed, it can be easily checked that $R_{ij}^P(\theta,\varphi) = \exp[-iH_{R^p}]$, with H_{R^p} in the $\{|d_i\rangle, |d_j\rangle\}$ subspace is given by

$$H_{R^p} = i\frac{\theta}{2} \begin{bmatrix} 0 & -e^{-i\varphi} \\ e^{i\varphi} & 0 \end{bmatrix}$$
 (B2)

which is exactly Eq. (A3) restricted to a single pair of eigenstates in resonance.

Starting from this, we can easily construct a universal set of logical single-qubit gates from logical planar rotations:

$$R_L^p(\theta,\varphi) = R^p(\theta,\varphi) \otimes I_{d/2} \tag{B3}$$

The corresponding effective Hamiltonian in the rotating frame has the following simple form in the logical bases:

$$H_{R_r^p}^{(l)} = H_{R^p} \otimes I_{d/2}.$$
 (B4)

To recover its form in the eigenbasis we perform the transformation

$$\tilde{H}_{R_L^p} = \mathcal{A}H_{R_L^p}^{(l)} \mathcal{A}^{\dagger} \tag{B5}$$

where we recall that \mathcal{A} is simply the set of code-words and error-words of the code. Thus imposing simple conditions on the structure on the elements of \mathcal{A} we can ensure that $H_{R_L^p}$ has zero diagonal and hence it can be implemented by a set of simultaneous pulses. For example, if we set d=4 and use the code words [72] as in the main text, then

$$\tilde{H}_{R_L^p} = \begin{bmatrix} 0 & 0 & h & 0 \\ 0 & 0 & 0 & h \\ \bar{h} & 0 & 0 & 0 \\ 0 & \bar{h} & 0 & 0 \end{bmatrix}$$

Appendix C: Fault-tolerant Two-qubit gates

In the logical bases, a generic two-qubit controlled logical gates CG can be defined similarly to logical single-qubit rotations introduced in the main text. Let us suppose CG is written as

$$CG = \begin{bmatrix} G_1 & 0 \\ 0 & G_2 \end{bmatrix}$$

then the gate defined by

$$CG_L \doteq \begin{bmatrix} I_{d/2} \otimes G_1 \otimes I_{d/2} & 0\\ 0 & I_{d/2} \otimes G_2 \otimes I_{d/2} \end{bmatrix}$$
 (C1)

is the logical representation of a controlled gate CG on two qubits, because it implements CG independently of the k of both the (logical) control and target. In our case we consider a logical $C-\varphi$, expressed in the logical two-qubit basis by the matrix

$$U_{C-\varphi} = \begin{bmatrix} 1 & 0 & 0 & 0 \\ 0 & 1 & 0 & 0 \\ 0 & 0 & 1 & 0 \\ 0 & 0 & 0 & e^{i\varphi} \end{bmatrix}.$$

1. Implementation on molecular spins

Fig. 5-(a) reports the circuit for the FT implementation of the controlled-phase gate $(C - \varphi)$ presented in the manuscript. To actually realize it on a real system, we consider the supra-molecule sketched in panel (b), consisting of three interacting logical qudits (LQs). For them we can assume a leading interaction of the form

$$H_{J} = \sum_{i,i',i''=0}^{d-1} \left[J\left(\frac{d-1}{2} - i\right) \left(\frac{d-1}{2} - i'\right) + J'\left(\frac{d-1}{2} - i''\right) \left(\frac{d-1}{2} - i'''\right) \right] |d_{i}^{(1)} d_{i'}^{(S)} d_{i''}^{(2)} \rangle \langle d_{i}^{(1)} d_{i''}^{(S)} d_{i''}^{(2)} |$$
(C2)

which could arise from a generic spin-spin exchange interaction between the qudits. Here $|d_i^{(1)}d_{i'}^{(S)}d_{i''}^{(2)}\rangle$ is the three-qudit $Q_1 - S - Q_2$ state. From Eq. (C2) we note that the energy needed to induce a logical excitation of the switch depends on the logical state of both Q_1 and Q_2 . This naturally arises from the definition of logical state $\ell = 0, 1$ on two disjoint subspaces [66].

We now clarify how a conditional phase on Q_1 , Q_2 can be obtained. The computational states of the two LQs Q_1 and Q_2 are defined in the subspace in which the switch is in $|\bar{0}\rangle$. The excited logical state of the switch $|\bar{1}\rangle$ is only exploited to implement the $C-\varphi$. In particular, a resonant rotation of the switch $R_L^P(2\pi,\phi)$ (i.e. $|\bar{0}\rangle \to |\bar{1}\rangle \to |\bar{0}\rangle$) yields a phase π on the component of the wave-function which is excited. Since such a rotation is implemented only for a specific $(|\bar{1}\bar{1}\rangle)$ state of Q_1 and Q_2 , this becomes a conditional phase into the computational subspace.

In a similar way, a generic phase $\varphi \neq \pi$ can be obtained if one implements a semi-resonant rotation of the switch, which corresponds to a pulse slightly detuned from the addressed energy gap, where the detuning controls the phase φ [71, 73].

The FT implementation of the C- φ gate follows immediately the all-to-all connectivity in the two-qubit bases, which follows from the all-to-all connectivity of each unit. Indeed, also this gate can be obtained starting from the zero-diagonal effective driving Hamiltonian $\tilde{H}_{C\varphi}$.

Appendix D: Stabilization, correction and encoding

We now turn our attention to the Fault Tolerant implementation of the stabilization process. Again, it turns out that the crucial requirement is the capability to directly implement planar rotations between any pair of qudit-ancilla eigenstates, i.e. to derive \tilde{H} for this process.

As reported in the manuscript, to detect an error k we propose a k-controlled operation CU between the logical qubit and an ancilla with d/2 levels initialized in $|0\rangle$. Such a controlled excitation can be realized by considering two qudits interacting with a Hamiltonian of the form (C2).

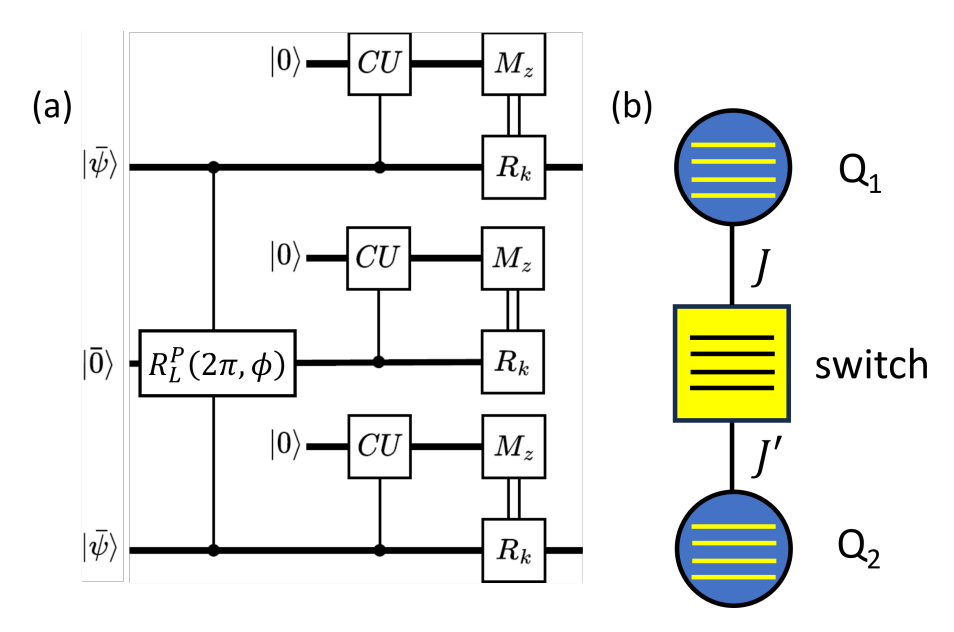


Figure 5: (a) Circuit for the implementation of a the Fault Tolerant two-qubit C- φ gate, followed by stabilization and measurement-dependent recovery. (b) Physical realization on a supra-molecular spin system consisting o three interacting spin qudits, where the middle one acts as a switch of the effective coupling between Q_1 and Q_2 .

As an example, we set d=4 and show the logical representation of the CU gate

while in panel (c) of Fig. 2 (main text) its schematized implementation in the eigenbasis.

In the same setting, the two recovery operators have the following logical representations

$$R_0 = \begin{bmatrix} 1 & 0 & 0 & 0 \\ 0 & 1 & 0 & 0 \\ 0 & 0 & 1 & 0 \\ 0 & 0 & 0 & 1 \end{bmatrix} \tag{D2}$$

$$R_1 = \begin{bmatrix} 0 & 1 & 0 & 0 \\ -1 & 0 & 0 & 0 \\ 0 & 0 & 0 & 1 \\ 0 & 0 & -1 & 0 \end{bmatrix}$$
 (D3)

and in panel (c) of Figure 2 (main text) is schematized the direct implementation of R_1 on the physical system.

Appendix E: Numerical simulations

In the simulations we have considered the system Hamiltonian introduced in Ref. [72], with the corresponding error model, codewords and errorwords. In particular, the examined molecular qudit consists of seven half-integer spins (six spins 1/2 and a spin 3/2), whose structure mimics the Ni₇ corner-sharing double tetrahedron [74]. The system is characterized by the spin Hamiltonian:

$$H = \sum_{i>j} J_{i,j} \mathbf{s}_i \cdot \mathbf{s}_j + \sum_{i>j} D_{i,j} (s_i^x s_j^y - s_i^y s_j^x) + \mu_B B \sum_i g_i s_i^z,$$
 (E1)

where the first leading term is the spin-spin isotropic exchange coupling, the second is the antisymmetric (axial) Dzyaloshinskii-Moriya interaction (DMI), and the last describes the interaction with an external magnetic field along z. The anti-ferromagnetic exchange couplings $J_{i,j}$, similar in magnitude and arranged as described in Ref. [72], give rise to a low-energy spectrum displaying several multiplets with total spin S = 1/2. The perturbative DMI term (combined with non-uniform g_i) then mixes these multiplets, giving rise to the all-to-all connectivity required by the scheme. We finally note that slight differences between the couplings in the spin Hamiltonian (E1) (typically occurring in real molecules with competing exchange interactions [75–80]) ensure that all the energy gaps are distinguishable and hence can be individually addressed by resonant pulses.

Time evolution of the system is described in the Lindblad approximation, by considering the interaction of the system with a markovian nuclear spin bath. Although more accurate descriptions of the bath dynamics would be possible given a set of nuclear spin coordinates [26], this does not qualitatively affect our results. Hence, we prefer to adopt a simplified and more general picture, regardless of the specific molecular structure, following Refs. [71, 72]. Within this framework, the dynamics of the system is computed by solving the quantum master equation

$$\dot{\rho} = -i[H_{rot}, \rho] + \underbrace{\sum_{n,m} \frac{\Gamma_{n,m}}{T_2} \left(2 \left| d_n \right\rangle \left\langle d_n \right| \rho \left| d_m \right\rangle \left\langle d_m \right| - \delta_{n,m} \left| d_n \right\rangle \left\langle d_n \right| \rho - \delta_{n,m} \rho \left| d_m \right\rangle \left\langle d_m \right| \right)}_{D(\rho)} \tag{E2}$$

and hence the differential equation is time independent and Γ_{mn} are system-specific dephasing rates. Switching to the superoperator formalism [81] $[H_{rot} \to \mathcal{H}, D \to \mathcal{D}]$ we can rewrite (E2) as

$$\frac{\partial}{\partial t} |\rho\rangle = \underbrace{\left[-i\mathcal{H} + \mathcal{D}\right]}_{\mathcal{F}[H]} |\rho\rangle$$

which has as a solution

$$|\rho\rangle(t) = e^{\mathcal{F}[H]t} |\rho\rangle(0).$$

In Eq. (E2), $|d_n\rangle$ are system eigenstates and the dissipator term $D(\rho)$ induces a decay of each off-diagonal element ρ_{mn} of ρ with a rate $\gamma_{mn} = \Gamma_{mm} + \Gamma_{nn} - 2\Gamma_{mn}$. The Γ_{mn} coefficients are given by:

$$\Gamma_{mn} = \sum_{jj'=1}^{N} C_{jj'}^{zz} \langle d_m | s_j^z | d_m \rangle \langle d_n | s_{j'}^z | d_n \rangle, \tag{E3}$$

where $C_{jj'}^{zz}$ depends on the molecular structure via the dipolar couplings between local system operators s_j^{α} and bath spin operators [72]. Note that here only $\alpha=z$ operators contribute due to the form of Hamiltonian (E1), but the extension to a more general case would be straightforward. For the simulations reported in the text we have introduced the effective dephasing time $T_2 = \left(\sum_{jj'} C_{jj'}^{zz}\right)^{-1}$, which includes information on the bath.

We finally note that that molecular spin qudits can be integrated within superconducting resonators which can be

We finally note that that molecular spin qudits can be integrated within superconducting resonators which can be used to readout the final state of the system and to mediate the interaction between different qudits or clusters of qudits, thus enabling to entangle different part of the register in a scalable architecture [68].

Appendix F: Measurements Errors

Ideal measurements on the d/2-levels ancilla are described by the projectors $P_k = |k\rangle \langle k|$. We model measurement errors at the end of the stabilization procedure by considering a deformation of the ideal projectors P_k as follows:

$$\Pi_k = (1 - p) |k\rangle \langle k| + \frac{2p}{d - 2} \sum_{j \neq k} |j\rangle \langle j|.$$

 Π_k represent a simple generalization to qudits of the "measurement operators" introduced in Refs. [64, 82]. This gives a probability 2p/(d-2) of being projected onto each eigenstate $|j \neq k\rangle$, given k as the measurement output. A different choice in the distribution of the "wrong projectors" does not alter our conclusions. For instance, by assuming a probability of being projected onto $|j\rangle$ which decreases with |j-k|, we find an even smaller impact of the measurement error.

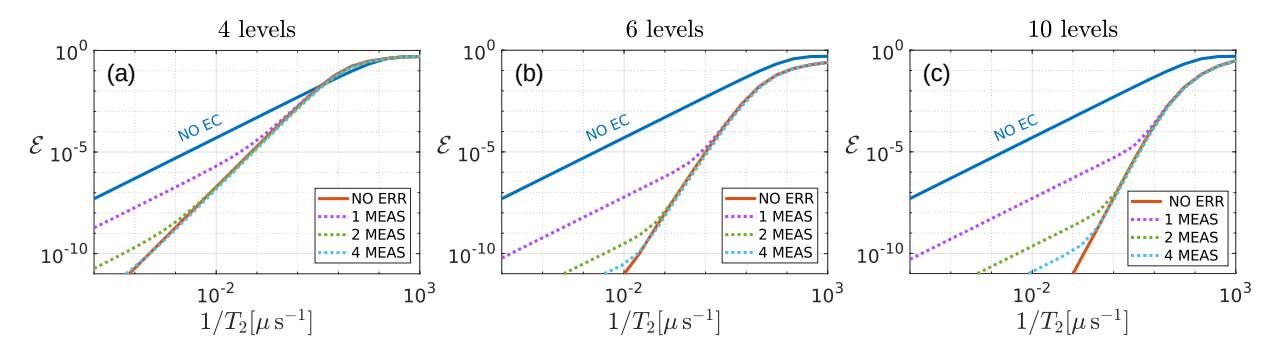


Figure 6: Comparison of the code performance with a measurement error probability p = 0.01 for a qudit with (a) 4, (b) 6 and (c) 10 levels. Dotted lines of different colors are obtained with n = 1, 2, 4 measurement repetitions, while continuous lines correspond to the case with no measurement errors (red) or no correction (blue). Clearly, measurement errors become negligible with a few measurement repetitions.

We first note that the recovery operation following a measurement error does not affect the state of the qudit. Indeed, suppose to have as measurement outcome k and to be projected onto $|j \neq k\rangle$. Then the qudit+ancilla state will be $(\alpha |0,j\rangle + \beta |1,j\rangle) \otimes |j\rangle$ and the recovery step R_k will be ineffective.

Hence, the measurement error can be suppressed by repeated measures of the ancilla, without needing to repeat the stabilization protocol [83]. In fact, after n repetitions, the measurement error probability $\sim p^n$ and hence can be made smaller than the error which is corrected by the code.

Below we report simulations of the FT error-correction procedure, including a measurement error with p=0.01. We note that after a few repetitions of the measurement at the end of the protocol we can reduce \mathcal{E} to an arbitrary extent, thus recovering the performance of the code with ideal measurements.